Linking CT and SPECT based analysis for quantitative follow-up of vascular perfusion defects in COVID-19

Catalin Fetita, Antoine Didier, Jean Richeux, Christian Tulvan, Jean-François Bernaudin, Aurelien Justet, Pierre-Yves Brillet

▶ **To cite this version:**

Catalin Fetita, Antoine Didier, Jean Richeux, Christian Tulvan, Jean-François Bernaudin, et al.. Linking CT and SPECT based analysis for quantitative follow-up of vascular perfusion defects in COVID-19. Medical Imaging, Computer-Aided Diagnosis, SPIE, Feb 2023, San Diego, United States. pp.124650E, 10.1117/12.2651945 . hal-04209804

HAL Id: hal-04209804
https://hal.science/hal-04209804v1

Submitted on 18 Sep 2023

HAL is a multi-disciplinary open access archive for the deposit and dissemination of scientific research documents, whether they are published or not. The documents may come from teaching and research institutions in France or abroad, or from public or private research centers.

L'archive ouverte pluridisciplinaire **HAL**, est destinée au dépôt et à la diffusion de documents scientifiques de niveau recherche, publiés ou non, émanant des établissements d'enseignement et de recherche français ou étrangers, des laboratoires publics ou privés.

Distributed under a Creative Commons Attribution - NonCommercial 4.0 International License

Linking CT and SPECT based analysis for quantitative follow-up of vascular perfusion defects in COVID-19

Catalin Fetita[1], Antoine Didier[1], Jean Richeux[2], Christian Tulvan[1], Jean-François Bernaudin [3,4,5,], Pierre-Yves Brillet[3,4] and Aurélien Justet[2]
[1]SAMOVAR, Télécom Sud-Paris, Institut Polytechnique de Paris, 91120 Palaiseau, France
[2]Pneumologie & Médecine Nucléaire CHU Caen, France
[3]Avicenne Hospital, AP-HP, Bobigny, France
[4]INSERM 1272 Université Sorbonne Paris Nord, Bobigny, France
[5] Sorbonne Université Paris

Abstract

COVID-19 still affects a large population worldwide with possible post-traumatic sequelae requiring long-term patient follow-up for the most severe cases. The lung is the primary target of severe acute respiratory syndrome coronavirus 2 (SARS- CoV-2) infection. In particular, the virus affects the entire pulmonary vascular tree from large vessels to capillaries probably leading to an abnormal vascular remodeling. In this study we investigated two modalities for assessing this remodeling, SPECT perfusion scintigraphy and computed tomography, the latter enabling the computation of vascular remodeling patterns. We analyzed on a cohort of 30 patients the relationship between vascular remodeling and perfusion defects in the peripheral lung area, which is a predominant focus of the COVID-19 infectious patterns. We found that such relationship exists, demonstrated by moderate significant correlations between SPECT and CT measures. In addition, a vascular remodeling index derived from the z-score normalized peripheral CT images showed a moderate significant correlation with the diffusing capacity of the lung for carbon monoxide (DLCO) measures. Altogether these results point CT scan as a good tool for a standardized, quantitative, and easy-to-use routine characterization and follow-up of COVID-19-induced vascular remodeling. An extensive validation of these results will be carried out in the near future on a larger cohort.

Keywords: vascular perfusion defects, vascular remodeling, lung perfusion scintigraphy, computed tomography, COVID-19

1. Description of purpose

COVID-19 pandemic continues to be a major concern worldwide, with the emergence of new variants of the virus keeping the medical community alert. The lung is the primary target of severe acute respiratory syndrome coronavirus 2 (SARS-CoV-2) infection, which ultimately may lead to severe hypoxia and death in the most critical cases of Coronavirus disease 2019 (COVID-19). In addition to gas exchange disruption due to acute alveolar and mesenchymal compartments injury, hypoxia is also consecutive to vascular alterations affecting the entire pulmonary vascular tree from large vessels to capillaries, as vasculitis and capillaritis respectively, frequently associated with microthrombi [1],[2].
Although endothelium is a major affected compartment during COVID-19, the vascular remodeling that persists during the chronic stages of COVID-19 needs to be better documented. Injected CT scan and SPECT are routine tools used to explore the lung vascular compartment, especially to rule out chronic or distal pulmonary embolism in patients with suspected pulmonary hypertension.
If vascular perfusion defects can be qualitatively assessed using perfusion scintigraphy (SPECT), such investigation still remains limited to specialized radiological centers, has higher cost than other modalities (including standard CT) and its interpretation is subject to inter-observer variability. Currently, perfusion defects are estimated based on the heterogeneity of the signal inside the lung but no quantitative measures are provided. This is partly due to the lack of normalization of the collected signal preventing for inter-patient comparison. On the other hand, standard CT is a modality largely available in clinical routine and has the advantage of the normalization of the Hounsfield values, allowing inter-patient comparative studies and differential diagnosis.
In this paper, we investigate:

(1) the possibility to standardize the interpretation of perfusion scintigraphy maps in the case of COVID-19 by focusing

on the peripheral lung regions known to be the most affected by the development of ground glass and fibrotic tissue and where vascular perfusion is easier to interpret because of the absence of large caliber vessels, and

(2) the possibility to predict perfusion defects from vascular remodeling patterns detected using standard CT investigation. By linking CT and SPECT analysis we may expect reducing the need of perfusion scintigraphy but also providing a way to a less invasive follow-up of the patients by exploiting the differential diagnosis allowed by CT.

2. Materials and methods

In this study, 30 patients were randomly selected from a retrospective cohort collected in 2021 at University Hospital of Caen, France, where COVID-19 patients suspected for vascular perfusion underwent CT and perfusion SPECT the same days. Functional data such as *diffusing capacity of the lung for carbon monoxide* (DLCO) were also collected and used as reference in our investigation.

2.1 Data preprocessing

For SPECT data, a rescaling of the signal value on a 16 bits range was performed in order to achieve a maximal visual contrast irrespective to the measured signal level. The linear rescaling coefficient was recorded for each exam to ensure the reconstruction of the original signal range if necessary. The 3D data was spatially resized to achieve an isotropic resolution of 1.2 mm in all directions.
The left/right lung masks were segmented from the scintigraphy data using a combination of hysteresis thresholding and morphological operations for shape regularization (Fig. 1). The 3D scintigraphy map and lung masks will be exploited as described later on to extract the perfusion 2D peripheral maps according to a cylindrical projection approach.

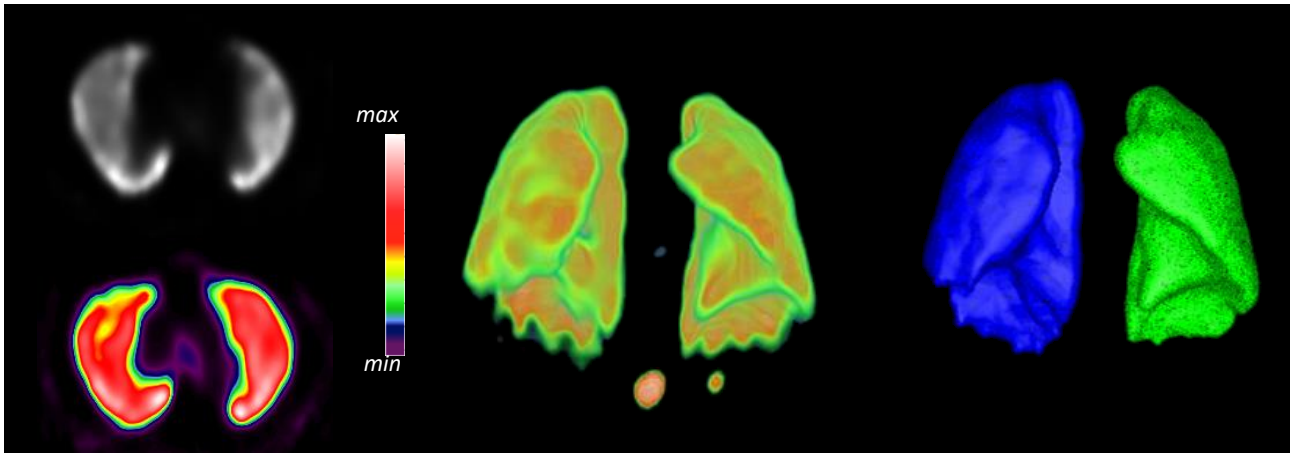

(a) (b) (c)

Fig. 1. Perfusion scintigraphy: (a) axial image (top – original, bottom – false colors), (b) perfusion volume data and (c) segmented lungs

The CT data was analyzed in order to build up a 3D vascular remodeling map accounting for both local vascular density and vessel caliber change. The original dataset was spatially resized to achieve an isotropic resolution of 0.6 mm in all directions. The 3D lung masks were segmented from the native CT data using a deep learning model with a UNet backbone, trained on a different database including control, idiopathic interstitial pneumonia and COVID (https://covid-segmentation.grand-challenge.org/COVID-19-20) subjects. The 3D vascular tree was reconstructed using the original approach of [3] upgraded in [4] to account for inter-subject CT protocol variability in the reconstruction of distal segments. The local vascular calibers were estimated at each point of the vascular tree using a morphological granulometric approach [5]. The interest of this approach is to allow identifying the region in a vascular segment corresponding to a given caliber range. This property will be exploited in computing the (local) ratio of blood volume of vessels with different cross-section sizes.

The segmented vascular calibers were used to compute a 3D vascular remodeling map as described in the following (Fig. 2). For each point in the 3D lung mask volume, two quantities are evaluated in a 3D region of interest (ROI) of 2x2x2 cm large:

- the ***local vascular density of small-to-medium caliber vessels (LVD)***. Larger caliber vessels are excluded from analysis since the remodeling we focus on appears to be limited to smaller vessels:

  $$LVD = BV20/V_{ROI}\,, \quad (1)$$

  where BV20 denotes the volume of blood vessels of cross-section area smaller than 20 mm^2 (radius < 2.5 mm) and V_{ROI} the volume of the ROI where BV20 is evaluated (i.e. 8 cm^3),

- the local blood volume ratio in the ROI, ***BV5/BV20*** (BVX denoting blood volume of vessels with cross section area less than X mm^2) accounting for the change in caliber.

The vascular remodeling map is defined at each point as the product of the above quantities, where low values correspond either to a low vascular density (vessel pruning) or to a shift in calibers from small to medium. The remodeling map is built-up using a stride of 2 in both axial and longitudinal directions, leading to an isotropic spatial resolution of 1.2 mm, as in the case of the scintigraphy maps. Note however that, in case of CT vascular remodeling map, both quantitative follow-up and inter-patient comparison is straightforward since the data is by default normalized, with the same meaning irrespective to the acquisition protocol, which makes it robust for follow-up studies (considering correct vascular segmentation and identical or similar lung inspiration volumes).

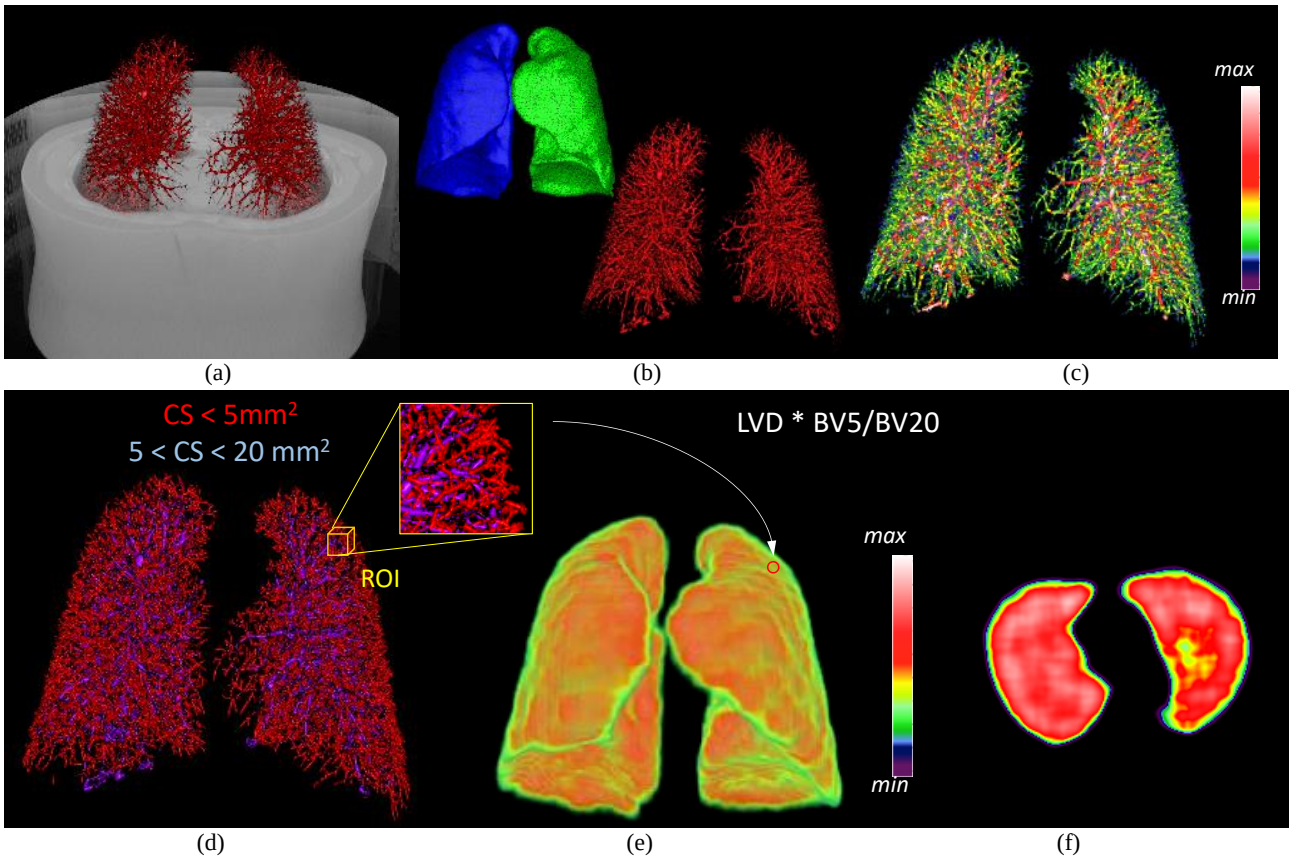

(a) (b) (c)

(d) (e) (f)

Fig. 2. CT analysis: (a) segmentation of native CT volume, (b) segmented lungs and vascular tree, (c) vascular calibers, (d) vessel tree partitioning according to the cross-sectional (CS) area and computation of vascular remodeling index in overlapping ROIs, (e) resulting 3D vascular remodeling map. (f) example of an axial slice of the vascular remodeling map

2.2 Peripheral mapping between vascular remodeling and perfusion defects

We hypothesize that the peripheral lung region is the most representative for studying both vascular remodeling and perfusion defects since large caliber vessels are not included and also because this region is known to be particularly affected by COVID infection (with ground glass and consolidation patterns shown at CT). Based on a previous study [4] and several experiments, we selected the width of the peripheral region of 3 cm.

For both SPECT and CT segmented lungs, we extracted the antero-postero-lateral lung periphery using the same following approach. First, the lung main axes in the axial plane are computed based on the apical-basal projection of the segmented lung volume (Fig. 3a – illustration for the right lung). For each axial image (Fig. 3b, white), the peripheral region is extracted as follows:
1- computation of the convex-hull of the lung (Fig. 3c),
2- dilatation of the convex-hull using a segment structuring element oriented in the lung short-axis direction towards the mediastinum (Fig. 3d)
3- erosion of the previous result using a disk structuring element of radius equal to the expected periphery width (Fig. 3e) and intersection with the lung section (Fig. 3f).

In order to provide a visual and a quantitative feed-back on the potential defects distribution in this region, we propose "unfolding" the lateral peripheral region according to a cylindrical projection applied in the axial short-axis (sagittal) direction for each lung, considering a 180° aperture angle with 0.5° between each projection ray (Fig 4). The value of a projection point in the resulting 2D image corresponds to the integral value along the projection ray.

Note that the projected peripheral maps may have lower (and thus inconsistent) values near the shape border since the width of the peripheral region corresponding to this area is smaller as it results from its construction (Fig. 3f).

(a) (b) (c) (d) (e) (f) (g)

Fig. 3. Definition of the antero-postero-lateral lung periphery at the level of an axial lung image (illustration for the right lung): (a) lung projection in the apical-basal direction and main axes computation, (b) individual slice (white) at mid lung height, (c) convex hull of b, (d) dilatation in the short-axis direction of c, (e) disk erosion of d, (f) difference d-e and intersection with b, (g) peripheral region (gray) of the lung slice (white).

Consequently, the ray integral across this region (Fig. 4b, red rays) will be smaller compared to medial regions (Fig. 4b, yellow ray). In order to reduce the bias of lower values on the border of peripheral maps, the map border of B pixels thickness is removed from analysis (the value of B=12 pixels is experimentally chosen based on visual inspection).

Another source of bias when comparing CT and SPECT peripheral maps will come from the different acquisition protocols. The CT data acquisition is obtained at full inspiration during the apnea, whereas the SPECT perfusion data is collected during free breathing in much longer time (around 20 minutes versus 5 seconds). This means that the SPECT data is averaged between inspiration and expiration maneuver compared to an instantaneous capture at inspiration for the CT. In order to limit the bias in comparing SPECT and CT maps, we apply an anisotropic smoothing to the CT peripheral map in order to mimic the inspiration motion. The Gaussian low-pass filtering takes into account the different lung motion amplitude in the axial versus sagittal direction by considering an horizontal smoothing with a kernel of 5 pixels radius and σ=2 and a vertical smoothing with a kernel of 20 pixels radius and σ=6. The resulting maps shown in Fig. 4c consider the above biases correction.

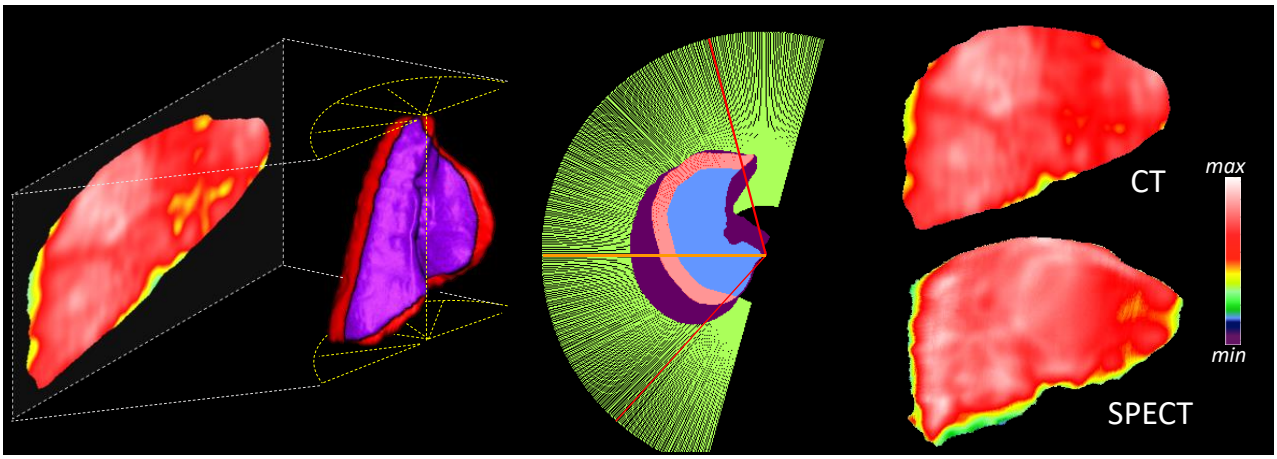

(a) Cylindrical medio-lateral projection of the peripheral region (red) of the right lung (blue)

(b) projection represented at the level of an axial image (as in Fig. 3). Ray integral across peripheral region (light red) will generate lower values on the shape border due to the reduced thickness

(c) Example of right lung peripheral maps obtained for vascular remodeling (top) and perfusion SPECT (bottom)

Fig. 4. Generation of lung peripheral maps by unfolding the lung peripheral region. Note that the color scale does not represent the same range for SPECT and CT.

2.2 Data analysis

Visual investigation of both perfusion and vascular remodeling peripheral maps indicates that the presence of perfusion defects as identified by radiologist expert on native axial SPECT images is depicted by lower values on these images (Fig. 5).

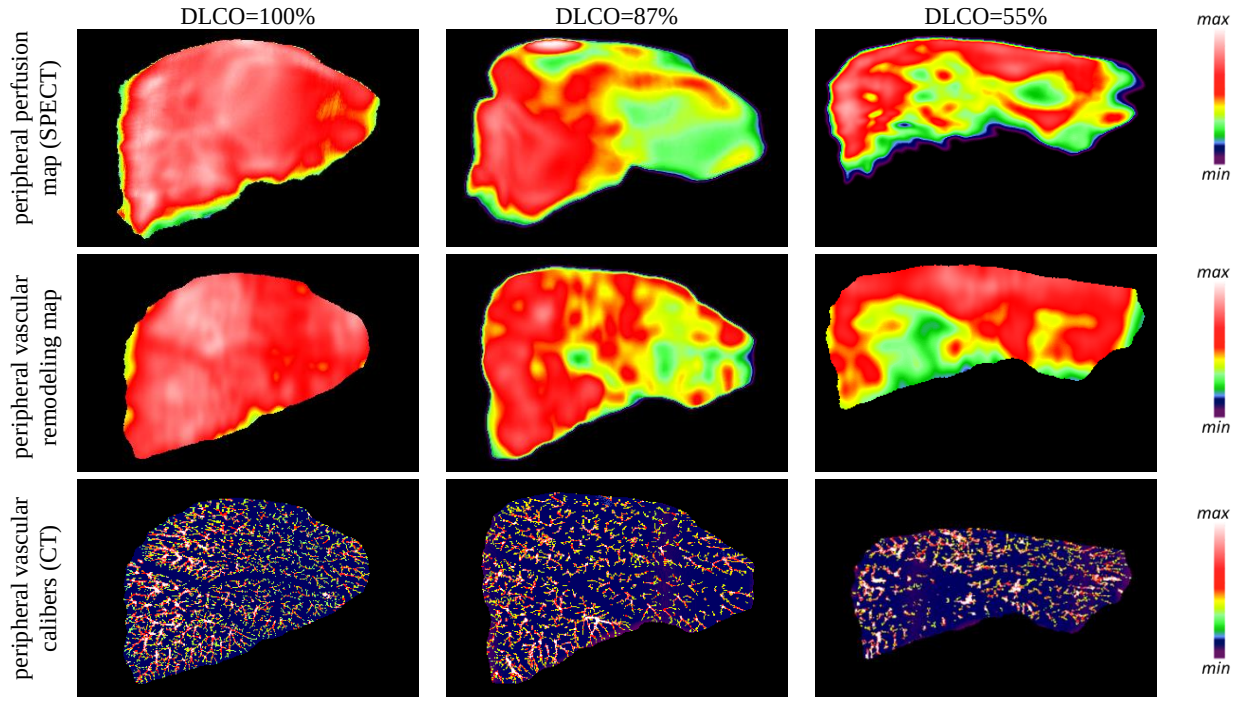

Fig. 5. Visual comparison of peripheral SPECT perfusion maps (top row, shown after registration), vascular remodeling maps (mid row) and peripheral vessels projections (bottom row) for three subjects: control (left), mild (middle) and moderate (right) perfusion defect. Note that the color scale does not represent the same range for SPECT and CT.

We analyzed existing correlations between SPECT peripheral perfusion and CT vascular remodeling maps to check the relationships between the two measures. In this respect, because perfusion SPECT is acquired in free breathing during a long period versus instant CT acquisition, the spatial extent of those maps is different. To account for this spatial shift, the perfusion map is registered on the CT vascular remodeling map using the approach in [6]. The resulting maps are partitioned in small ROIs (15x15 pixels) and the Pearson's correlation coefficient is estimated between the average values inside these ROIs.

Second, we investigate if the vascular remodeling analysis performed in CT can be predictive of perfusion defects in SPECT. For this, the defect detection is based on the z-score normalization of the two maps and considers as abnormal any region in the map where the z-score is smaller than a given threshold. This latter is empirically set-up at -0.2 based on the visual analysis of the peripheral maps (Fig. 5 top-middle rows) in conjunction with the peripheral projection of the vascular calibers in the same region, as segmented from CT (Fig. 5 bottom row). The abnormal region selected be the z-score threshold should simultaneously correspond to decreased values in the peripheral maps and to visible disorders in peripheral vascular projections (pruning or caliber increase). Fig. 6 illustrate the abnormal regions detected for the cases in Fig. 5.

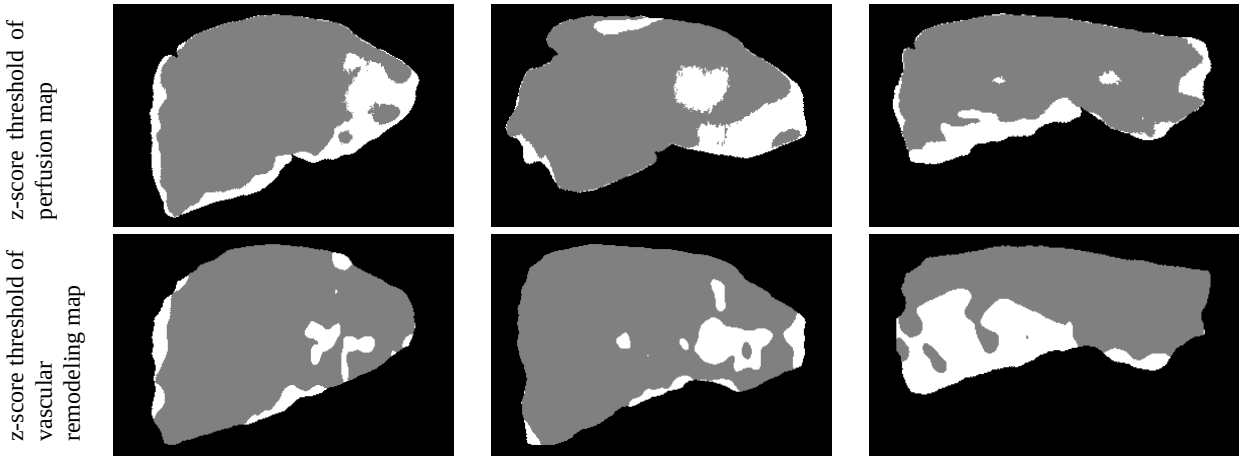

Fig. 6. Definition of abnormal regions in peripheral maps based on z-score value (subjects of Fig. 5).

In order to assess if a remodeling defect detection in CT vascular map can predict a corresponding defect in the perfusion map, we defined the detection rate of perfusion defects in SPECT by CT analysis, $R_{pred}^{CT\text{-}SPECT}$, as the Dice score computed between the suspicious regions in SPECT and the same regions selected by the suspicious regions in CT (Fig. 7). We also report the Dice coefficient between abnormal regions in CT and SPECT z-score maps as additional information on region matching.

Third, we analyze possible correlations between different measures derived from the unfolded peripheral maps of CT / SPECT and the DLCO values recorded for the patients in our cohort. A ***peripheral perfusion (resp. vascular remodeling) index (PPI / PVRI)*** is computed as the average value of these maps (lower values indicating higher defects). A ***perfusion* (SPECT) / *vascular* (CT) *defect score*** is defined based on the z-score maps (Fig. 6) as the ratio of the abnormal region surface (white) versus the total map surface (gray and white). These defect scores are further referred to as ***def_SPECT*** and ***def_CT***, respectively.

3. Results and discussion

We found a moderate significant correlation at the patient level between the peripheral perfusion and vascular remodeling maps (average $\rho = 0.51$, standard deviation = 0.12; median = 0.52) showing an existing quantitative relationship between vascular remodeling assessed with CT and perfusion defects shown in SPECT (Fig. 8).

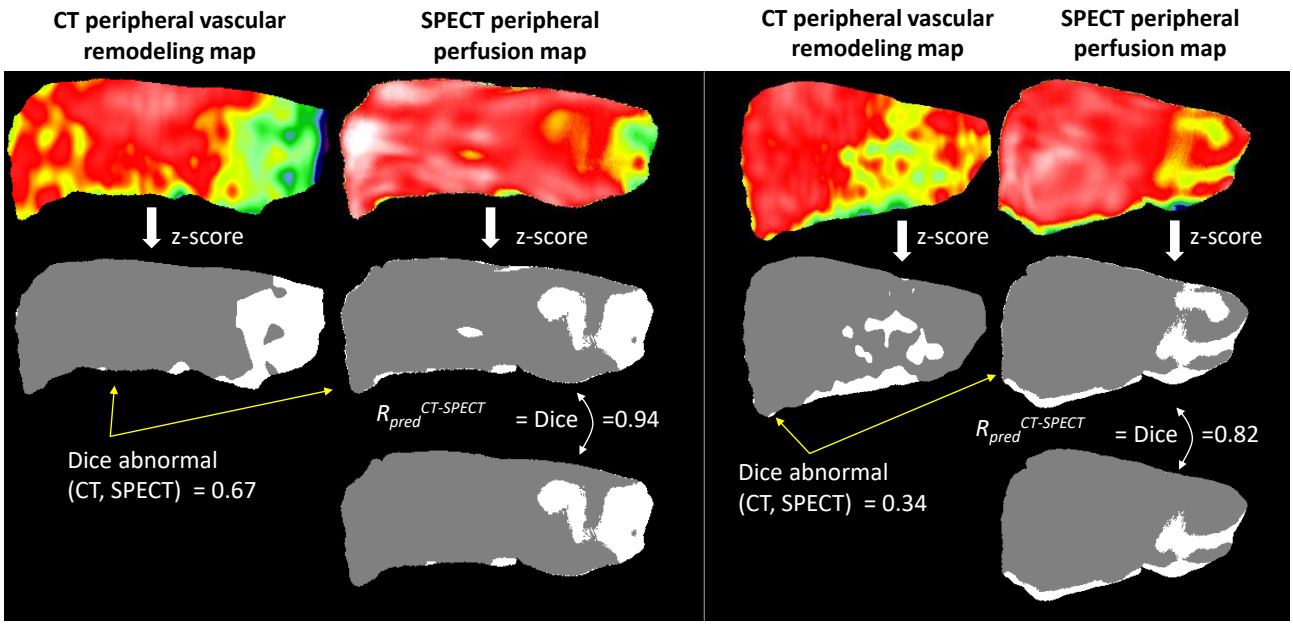

Fig. 7. Computation of the predictive score of abnormalities in SPECT perfusion map from CT vascular remodeling map for two cases. In each column, the bottom-row image represents the reconstructed abnormalities of SPECT z-score map from the CT z-score map.

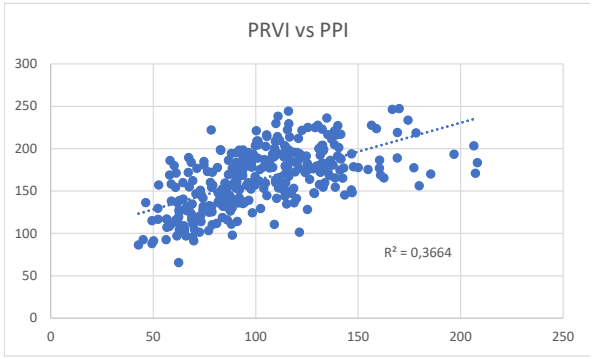

ρ=0.6
p < 0.001

correlation plot

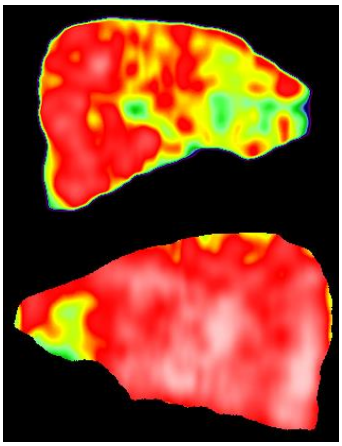

PVR maps for right (top) and left (bottom) lungs

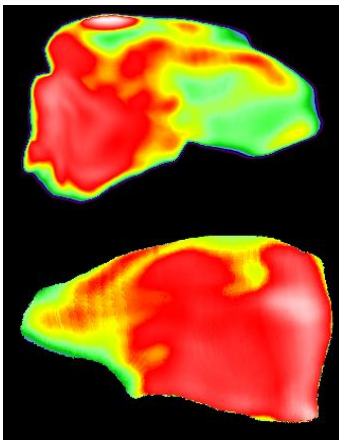

PP maps for right (top) and left (bottom) lungs

Fig. 8. Example of correlation between peripheral vascular remodeling (PVR) maps and peripheral perfusion (PP) maps values computed in ROIs of 15x15 pixels for both lungs (patient Fig. 5 middle column).

The analysis on the ability of peripheral vascular remodeling map from CT to predict perfusion defects visible in peripheral SPECT perfusion map shown an average predictive score $\boldsymbol{R_{pred}^{CT\text{-}SPECT}}$ = 0.95 (standard deviation = 0.05; median value = 0.96). Note that $\boldsymbol{R_{pred}^{CT\text{-}SPECT}}$ does not account for the overlapping percent between abnormal regions depicted by the z-score threshold in CT and SPECT peripheral maps (Fig. 7) but only for the detection ratio of these regions in SPECT by CT and the extent of these versus missed abnormal regions in SPECT. In order to measure the region matching in terms of surface, we computed the Dice score between the abnormal regions detected in CT and SPECT. We found an average Dice coefficient of 0.42 (standard deviation =0.12; median value = 0.43) which can be expected given the regional correlation values of PVR and PP maps. An in-depth investigation we plan to perform in the future is an analysis with respect to the z-score threshold selection for the peripheral perfusion map, which could be different from the one for the peripheral vascular remodeling map.

The analysis of correlation between the vascular remodeling / perfusion defect score (*def_CT* / *def_SPECT*) and the DLCO value has shown a significant moderate negative correlation for *def_CT* and a non-significant negative low correlation for *def_SPECT* (Fig. 9). Again, the z-score threshold selection for the peripheral perfusion map can be questioned in regard with these results; however, they underline the effectiveness of the CT-based quantification of vascular defects.

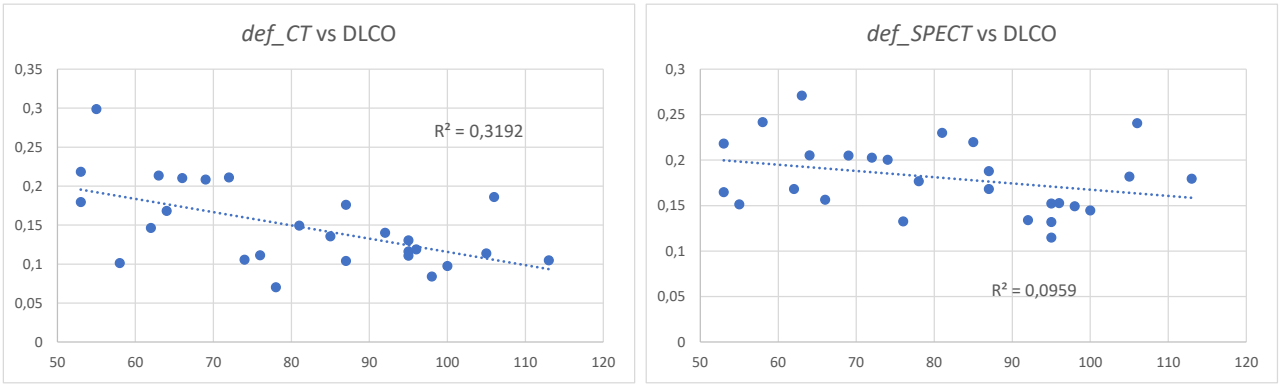

ρ= -0.565, p=0.002 ρ= -0.31, p=0.116

Fig. 9. Correlation between DLCO and the vascular remodeling / perfusion defect scores.

Interestingly, a low non-significant correlation with DLCO (ρ = 0.2) was found for both peripheral vascular remodeling index (PVRI) and peripheral perfusion index (PPI). This is somehow unexpected, especially for PVRI, considering the significant moderate correlation between *def_CT* and DLCO, the *def_CT* score being derived from the PVR map. This is explained by the fact that the PVRI value does not take into account the lung volume; the local vascular density (LVD, eq. 1) being computed with respect to the same ROI volume (8 cm^3), it is affected by the lung inflation (lower vascular density for higher lung inflation). When PVRI is corrected by lung volume (PVRI values multiplied by the lung volume), a significant moderate correlation ρ=0.48 (p=0.011) is found between corrected PVRI and DLCO (Fig. 10). Such correction is obtained by default for the z-score computed from the PVR map, which explains the significant correlation between *def_CT* and DLCO.

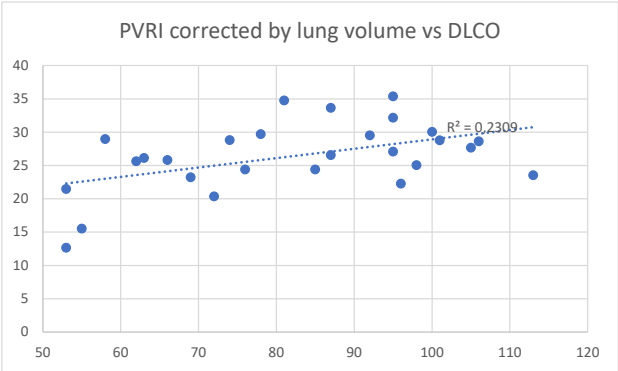

Fig. 10. Correlation between lung volume-corrected PRVI and DLCO (ρ=0.48, p=0.011).

Note that a similar correction cannot be applied to perfusion SPECT data (PPI) since this data is acquired during several breathing cycles. In addition, SPECT is a qualitative assessment modality and inter-patient normalization is not trivial and may involve in-depth knowledge on the tracer injection.

These results show that CT can be considered as a modality for quantitative assessment and follow-up of vascular remodeling in relation to COVID-19-induced perfusion defects.

4. Conclusion

This paper investigated the relationship between vascular alterations in COVID-19 assessed respectively with perfusion

scintigraphy (SPECT) and standard CT and showed that vascular remodeling evaluated on the peripheral lung region in CT can predict the occurrence of perfusion defects as depicted by SPECT. This could provide a standardized, quantitative, more versatile and robust alternative for characterization and follow-up of vascular defects in COVID-19. Such analysis, which is widely available, could be used in conjunction with the perfusion SPECT study to provide quantitative feedback of the examination interpretation, but also as a preliminary step to decide the need for an additional SPECT study. Work is currently underway to expand the inclusion of patient data in the study to achieve full validation of the current results.

Acknowledgement

This study was funded by the Fondation du Souffle, France, and by the ANR-20-COV4-0004 project (Silicovilung).

References

1. Synn AJ, Li W, Estépar RSJ, Washko GR, O'Connor GT, Tsao CW, Mittleman MA, Rice MB, Pulmonary Vascular Pruning on Computed Tomography and Risk of Death in the Framingham Heart Study, AJRCCM, sept. 2020, 0.1164/rccm.202005-1671LE
2. Lins *et al*., Assessment of Small Pulmonary Blood Vessels in COVID-19 Patients Using HRCT, Academic Radiology, Vol 27, No 10, October 2020, https://doi.org/10.1016/j.acra.2020.07.019
3. A.F.Kouvahé, C.Fetita, "A Generic Approach for Efficient Detection of Vascular Structures", IRBM 2020, https://doi.org/10.1016/j.irbm.2020.06.011
4. Fetita C. *et al*, Multiparameter analysis of vascular remodeling in post-acute sequelae of COVID-19, Proceedings Volume 12033, Medical Imaging 2022: Computer-Aided Diagnosis; 120330A (2022) https://doi.org/10.1117/12.2611461
5. Fetita C., *et al*, "Airway shape assessment with visual feed-back in asthma and obstructive diseases", in Medical Imaging 2010: Visualization, Image-Guided Procedures, and Modeling, Proceedings of SPIE Vol. 7625, p. 76251E:1-12
6. Fetita C. *et al*., "Diffusion-based interpolation with geometrical constraints applied to investigation of interstitial lung diseases", 2020 IEEE 20th International Conference on Bioinformatics and Bioengineering (BIBE), 10.1109/BIBE50027.2020.00106